

living planet symposium

BONN
23–27 May
2022

TAKING THE PULSE
OF OUR PLANET FROM SPACE



**MACHINE LEARNING BASED APPROACH
FOR SATELLITE DETECTION OF POTENTIAL NEW ARCHAEOLOGICAL SITES
LINKED TO THE MOBILITY OF PREHISTORIC GROUPS IN THE EGYPTIAN WESTERN DESERT**

Alessia Brucato, Nicola Masini, Giuseppe Scardozzi, Giulio Lucarini

D2.12.1 Cultural and Natural Heritage – 1
Room H2-02

26/05/2022

ENVIRONMENT

ARCHAEOLOGICAL CONTEXT

WORKFLOW

PLATFORMS

PARAMETERS

IMAGE PROCESSING

ALGORITHMS

REFERENCES

INTRODUCTION

MATERIALS

METHODS

RESULTS

CONCLUSIONS

ENVIRONMENT

SITES

SLAB STRUCTURES

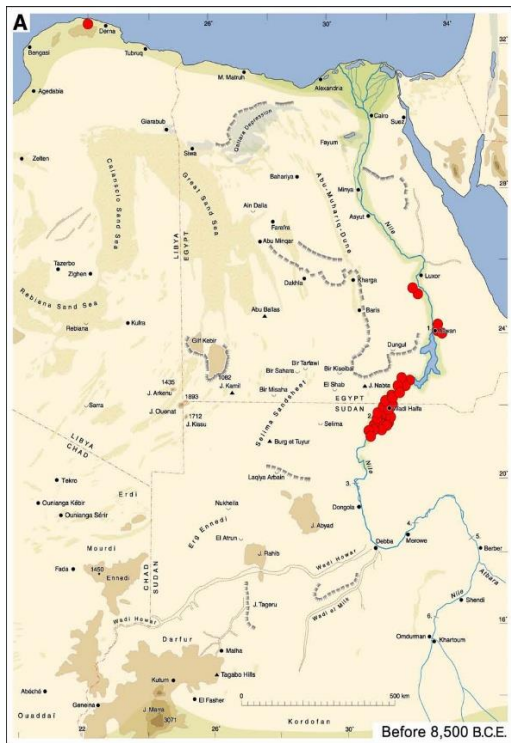
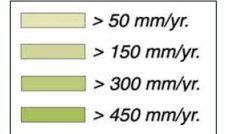
DATASET

IMAGERY

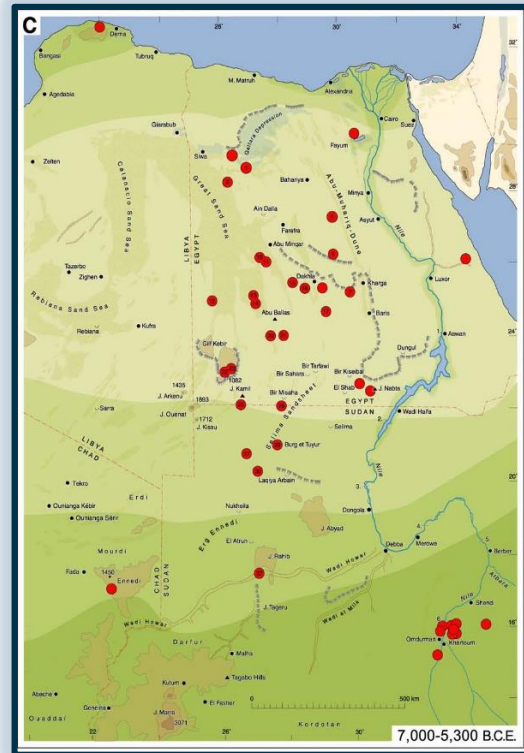
PRELIMINARY RESULTS

Holocene climatic sequence of the Eastern Sahara

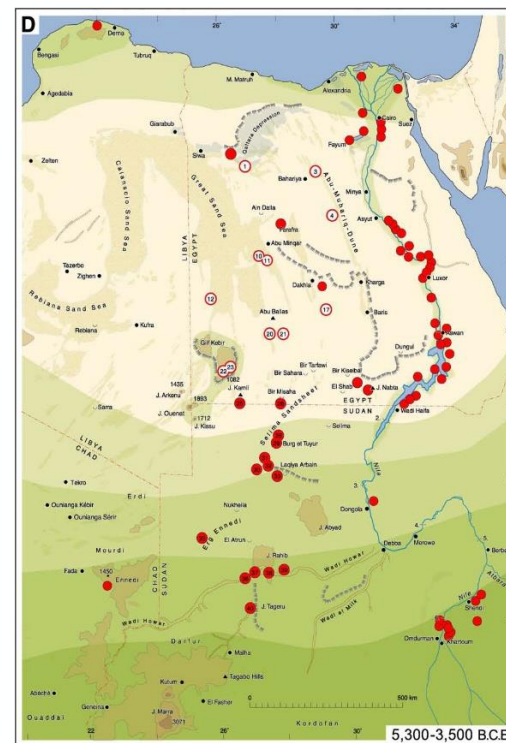
(Kuper, Kröpelin 2006)



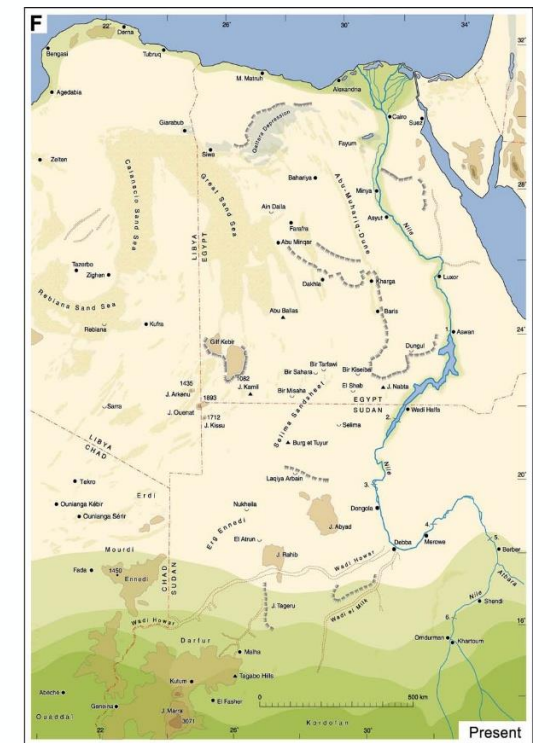
Before 8500 BC



7000-5300 BC



5300-3500 BC



Today



Early Wadi el Obeiyid A

6600-6100 cal. BC

- **Increased Sedentism**
- Structured hearth pits
- *Steinplätze* hearths

Sites: Hidden Valley IIIA, El Bahr



Late Wadi el Obeiyid A

6100-5700 cal. BC

- **Semi-permanent settlements**
- First slab structures
- Structured hearth pits

Sites: Hidden Valley Village III, IIA, Sheikh el Obeiyid Village



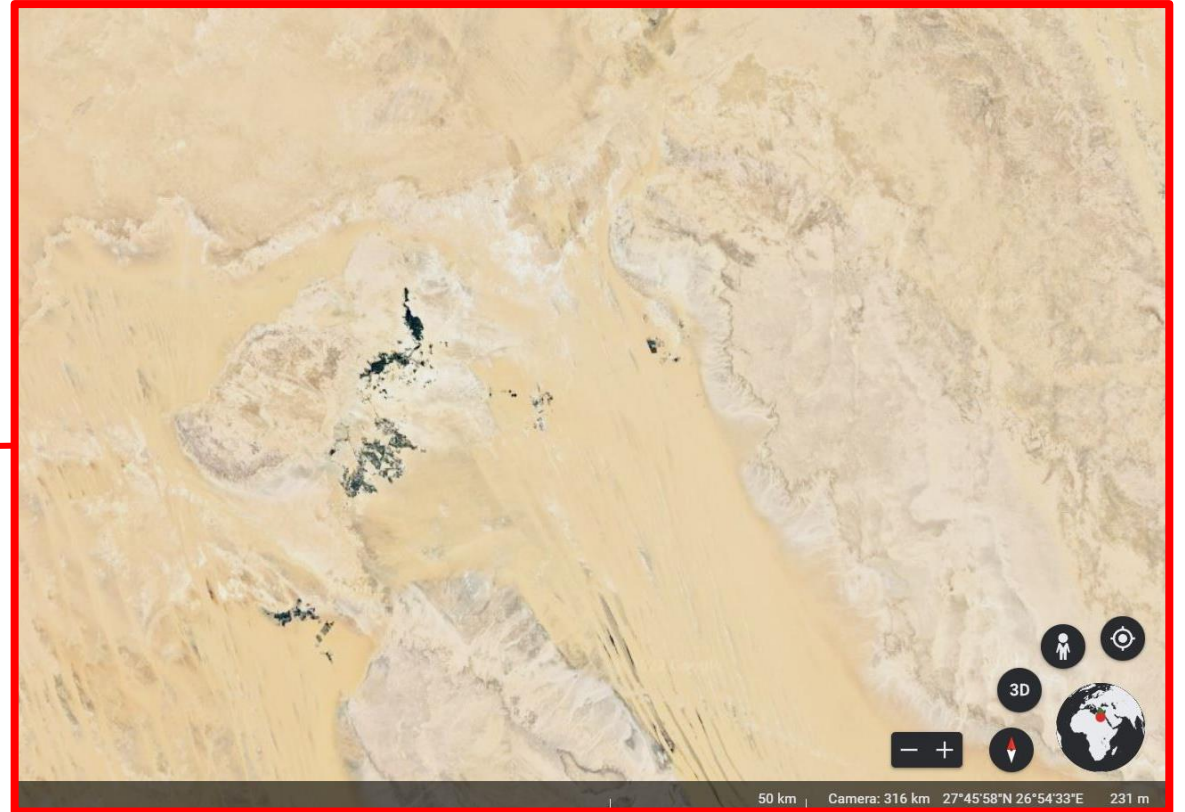
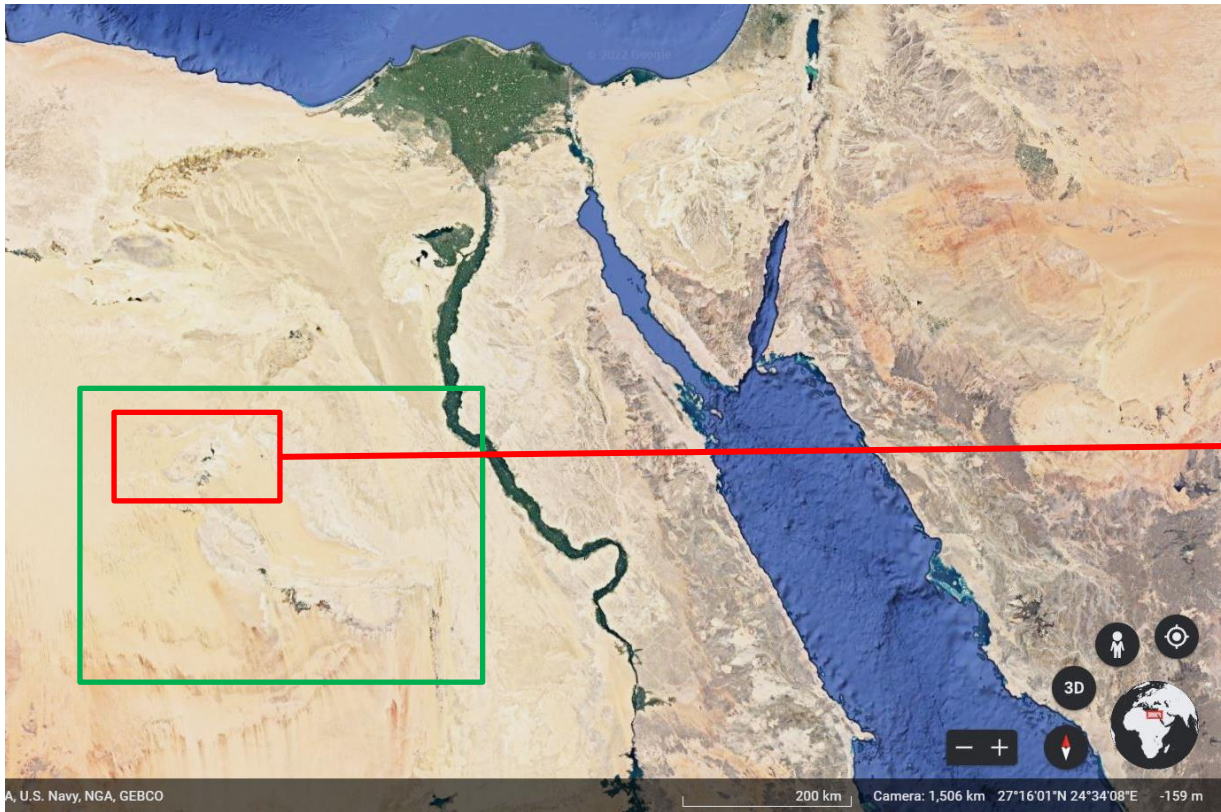
Wadi el Obeiyid B

5600-5200 cal. BC

- **Seasonal movements**
- Slab structures
- *Steinplätze* hearths

Sites: Hidden Valley II, El Bahr – Bir el Obeiyid

Oases of the Egyptian Western Desert Farafra Oasis

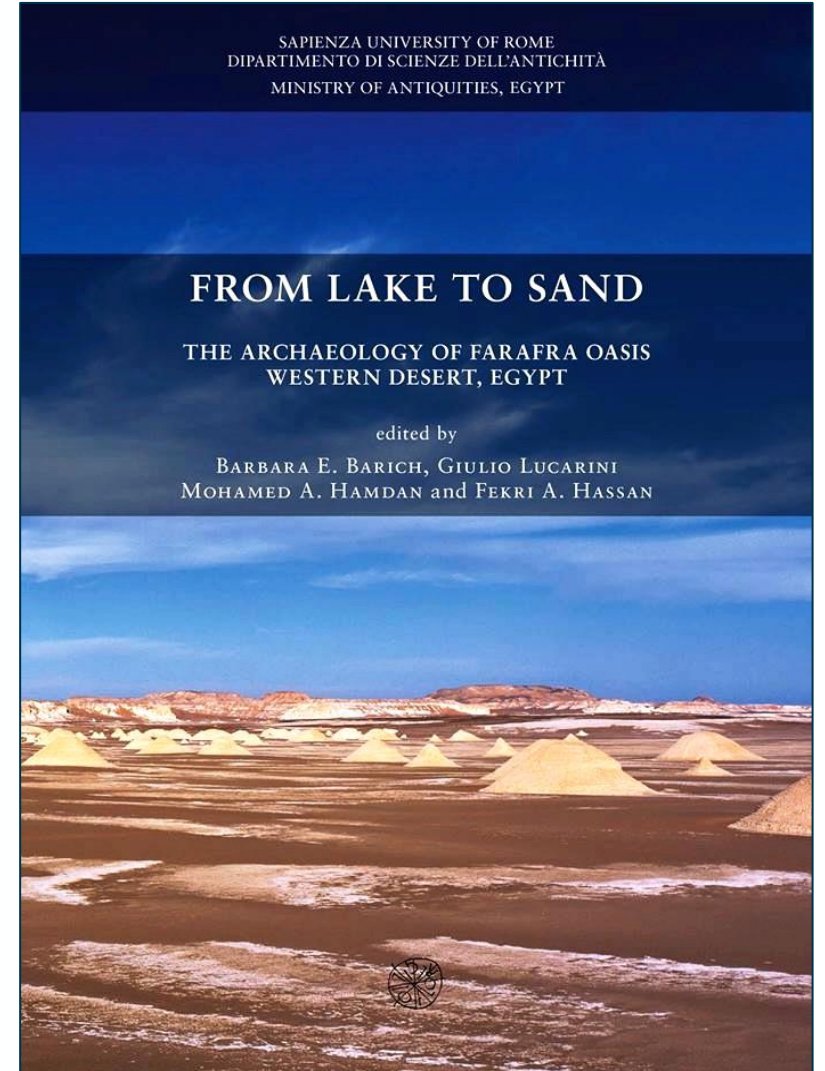


Farafra Oasis Prehistoric Project

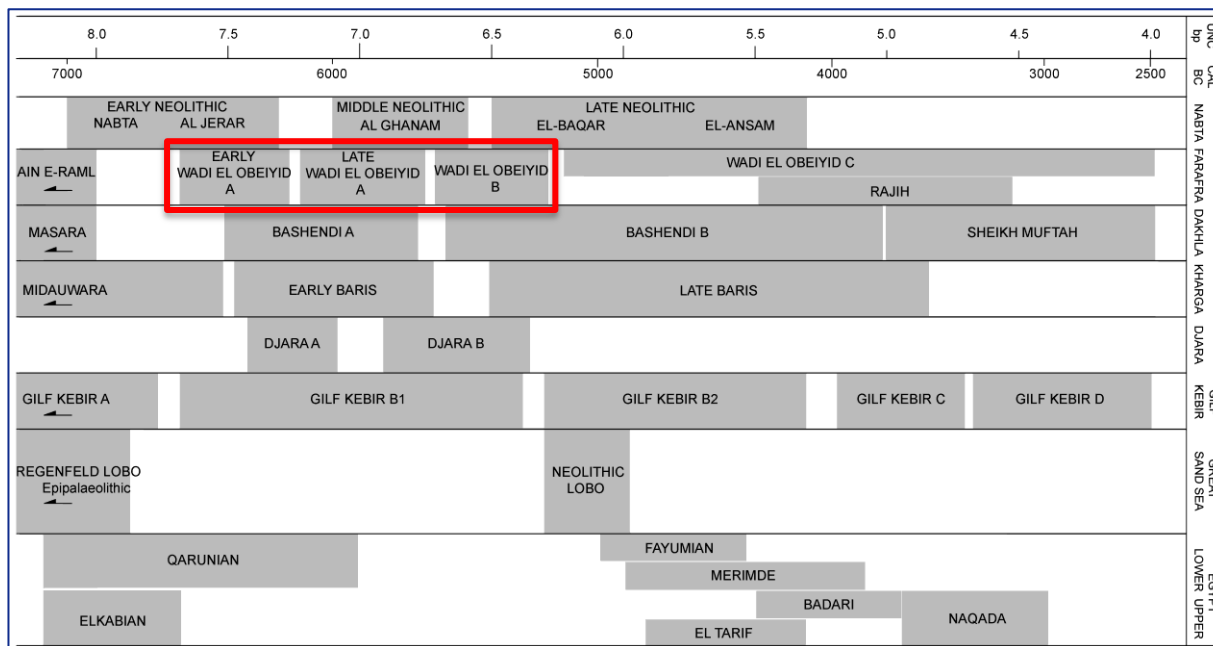
Co-directors: Barbara E. Barich, Giulio Lucarini

Egypt, since 1986

https://www.ismeo.eu/portfolio_page/italian-archaeological-mission-to-the-farafra-oasis-western-desert-egypt/



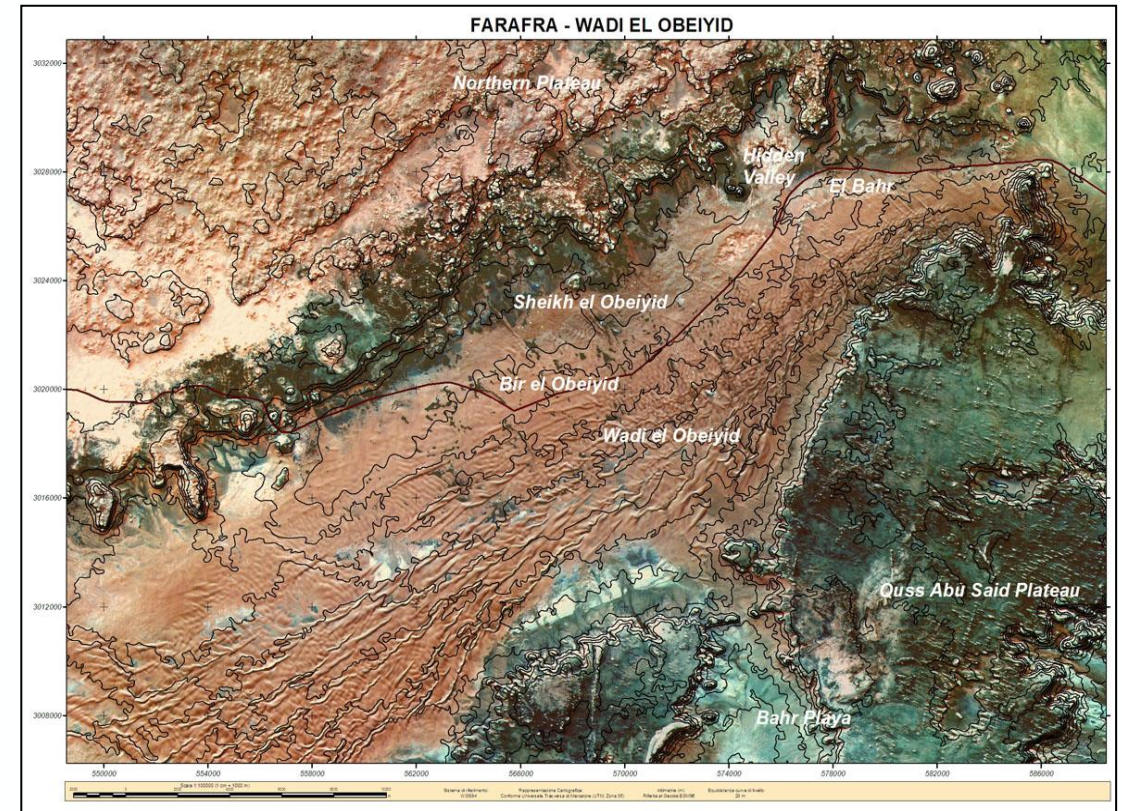
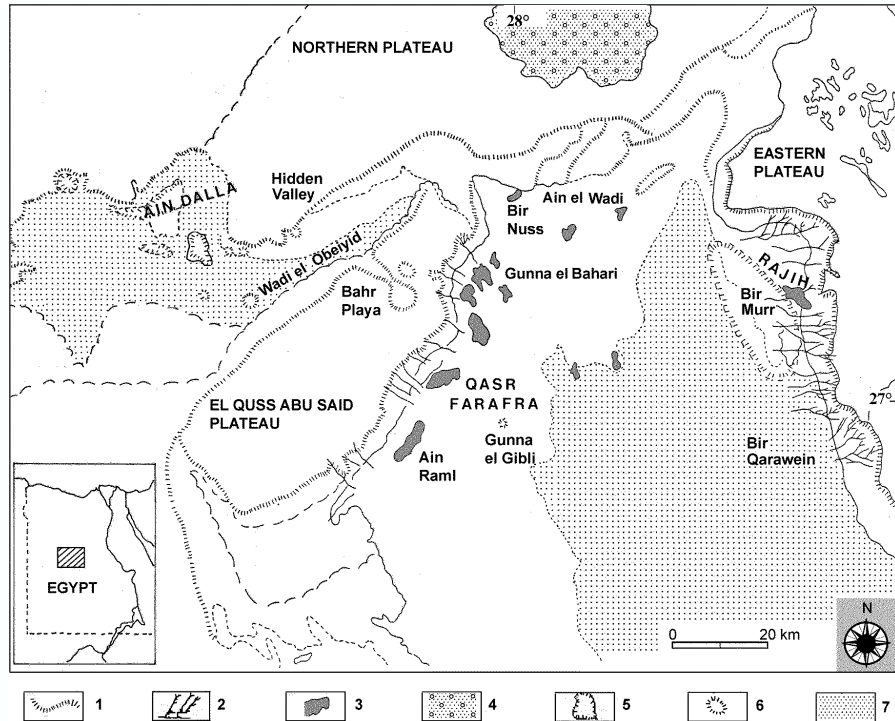
Mid Holocene Wadi el Obeiyid A-B 6600-5200 BC Foragers/herders



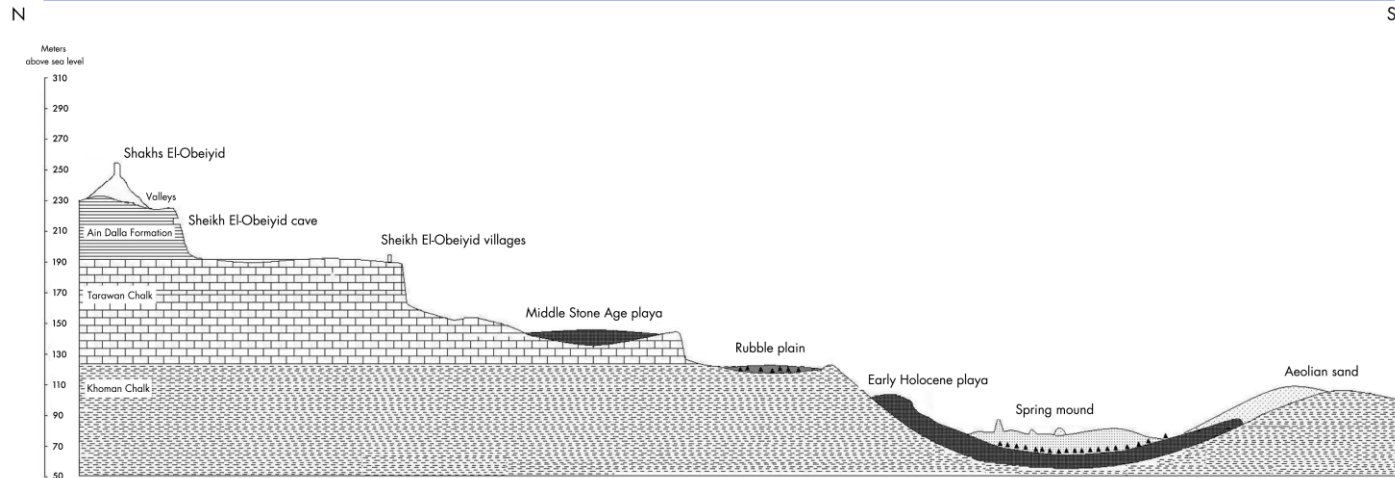
Mohamed A. Hamdan

Date BP	Unit	Palaeoenvironment		Climate	Archaeology	
		North	South			
< 4500		Desert wind erosion and aeolian deposit accumulation	Basinal	Desert wind erosion and formation of yardangs and aeolian deposits accumulation	Hyper arid	(?)
5000 to 6000	V	Wadi activity and colluviums		Playa basinal silt deposition (wadi fed playa)	Moist	Late Neolithic artifacts, hearths and ostrich eggshells
ca 6000	IV	Wind blown accumulation with few torrential floods		Dryness of the playa, wind deflation and phytogenic dune accumulation	Arid	Final occupation of the Neolithic village
6000 to 7000	III	Beach sand and gravel and at least 10 high stand lake		Playa basinal silt deposition (wadi fed playa)	Wet	Neolithic occupations at the Hidden Valley village, stone structures, flint implements, ostrich eggshell
ca 8000	II	Wind blown accumulation and alluvial and colluvial activity		Sheet wash and slope wash accumulation in the basin (wash playa)	Frequent dry	Hearths
> 8000	I	Wadi activity, sand and gravelly beach few high stand lakes and colluvium		Playa basinal silt deposition and few alluvial activity (wadi fed playa)	Wet	Final Palaeolithic (LSA) on top of lower plateau

Mid Holocene Wadi el Obeiyid A-B 6600-5200 BC Foragers/herders



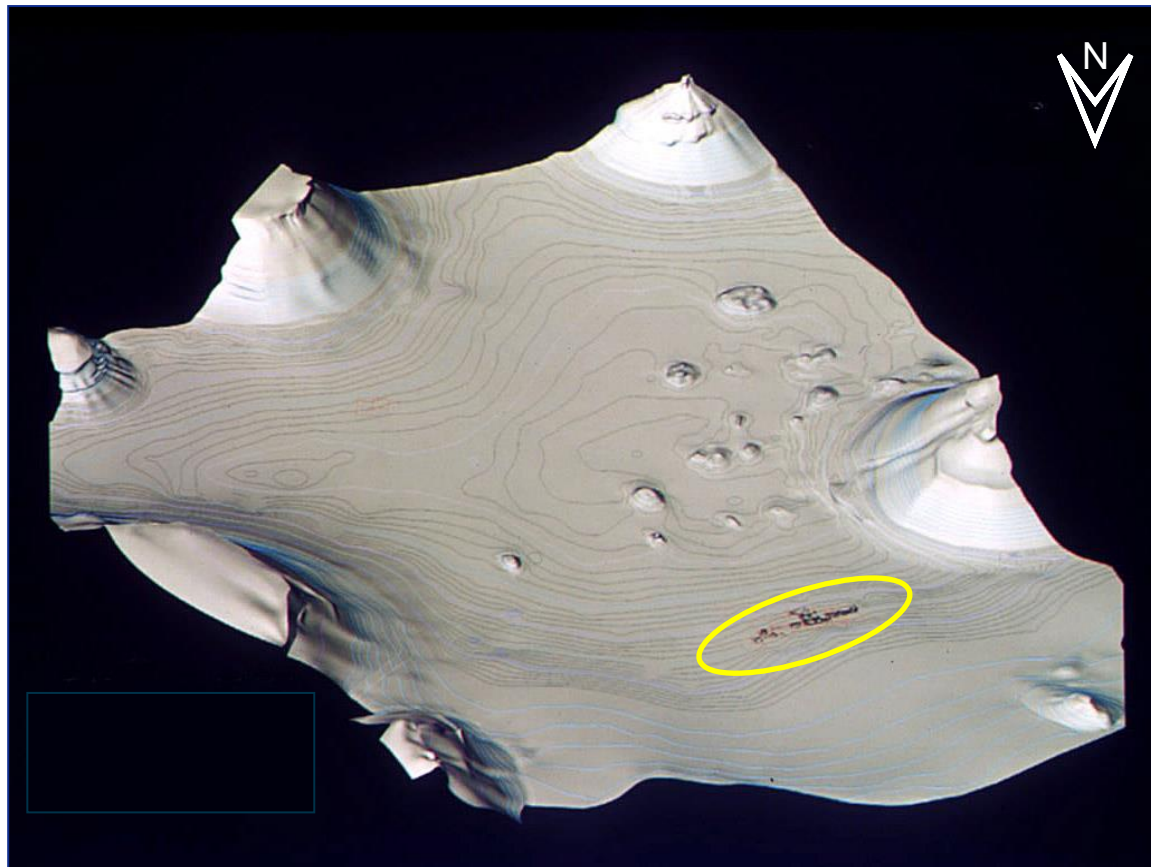
Ulisse Fabiani



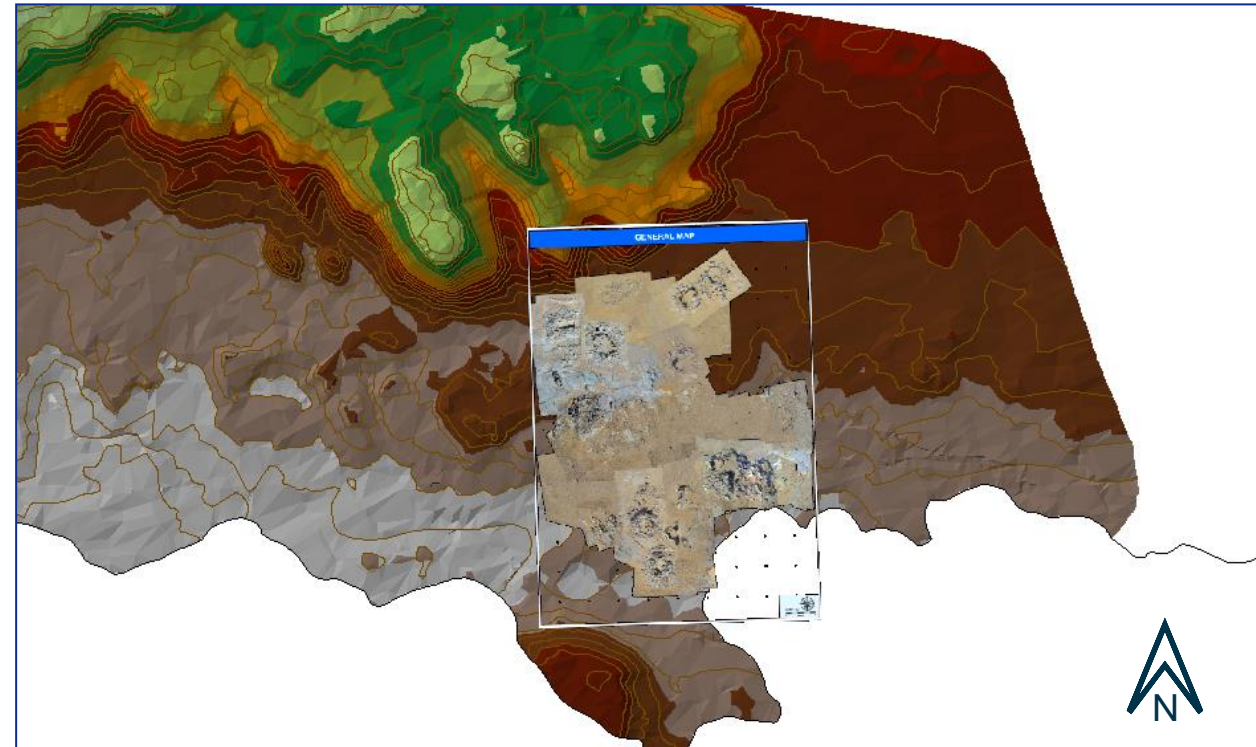
Mohamed A. Hamdan

Wadi el Obeyid Northern Plateau

Hidden Valley basin and village

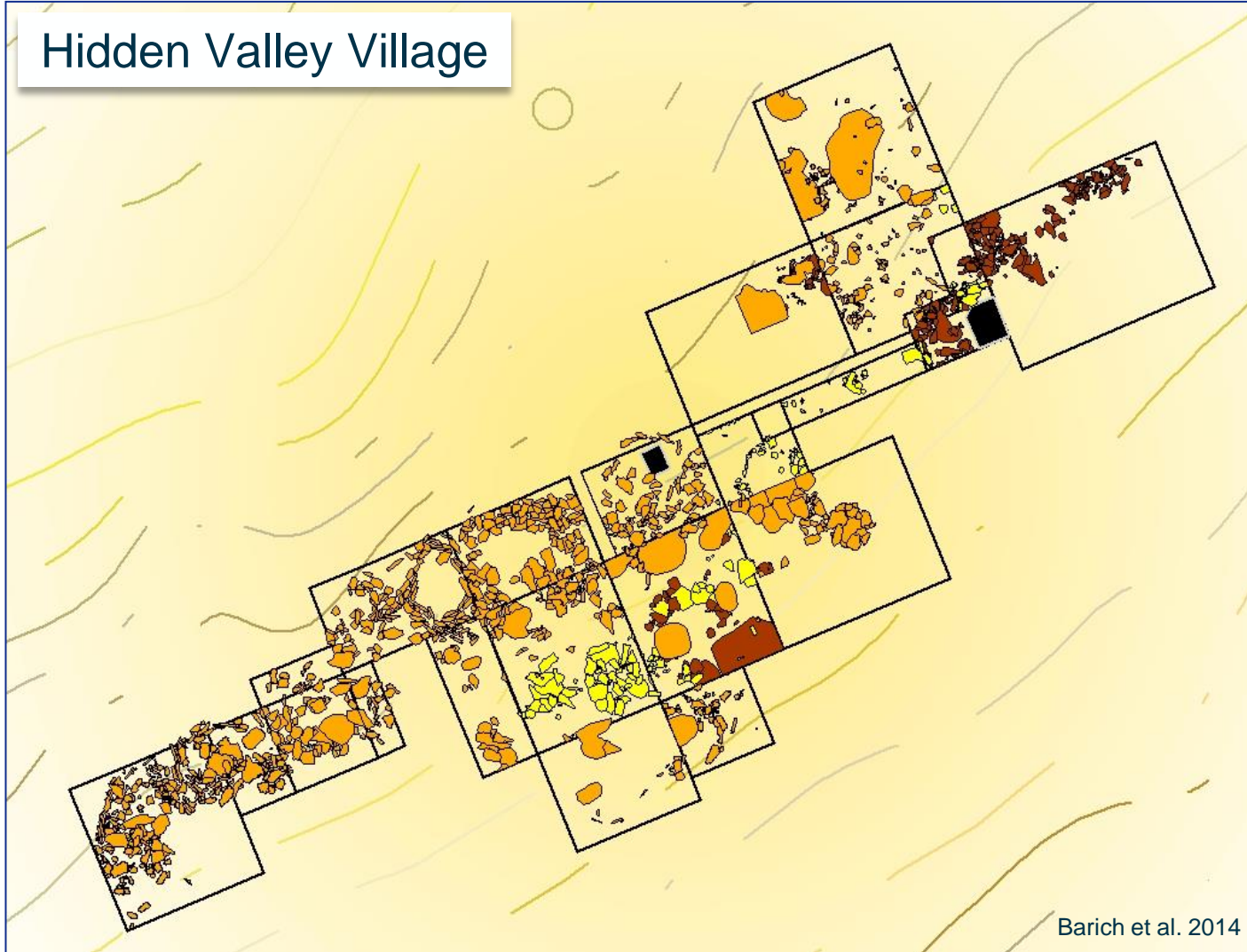


Sheikh el Obeiyid Village

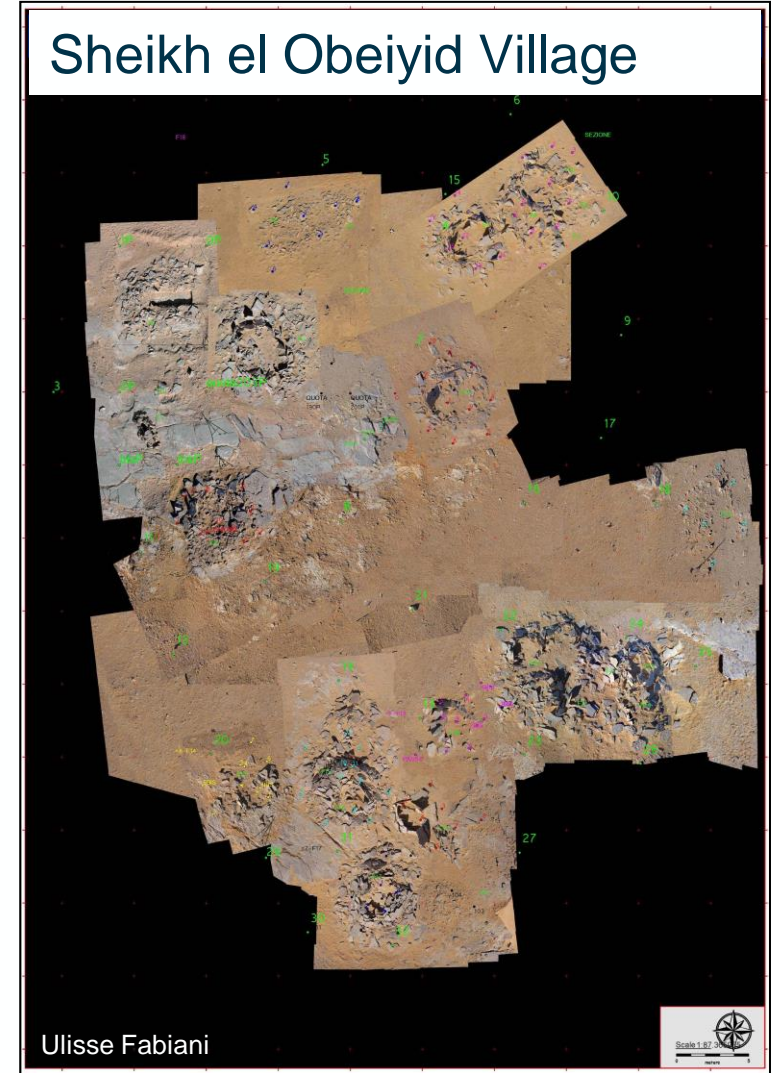


Ulisse Fabiani

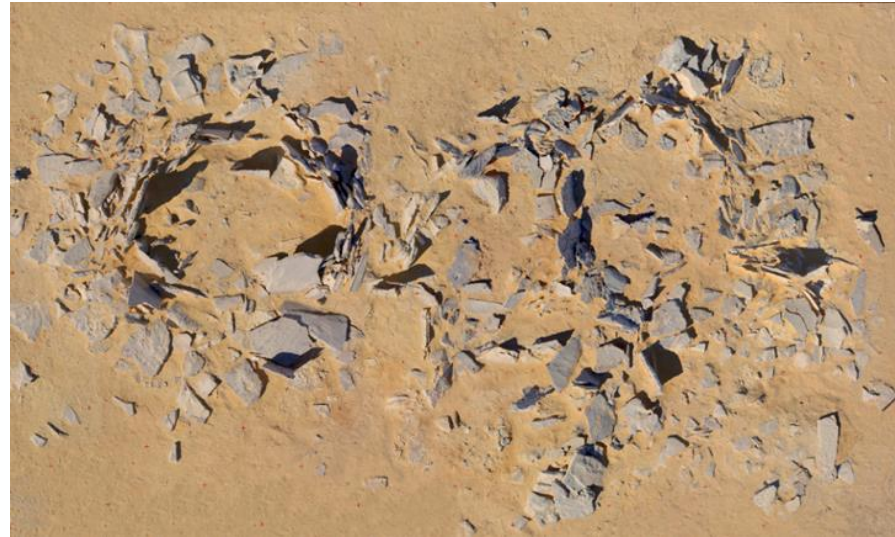
Hidden Valley Village



Sheikh el Obeiyid Village



MATERIALS – SLAB STRUCTURES



Fabrizio Galeazzi

SATELLITE IMAGERY

Corona KH-4B

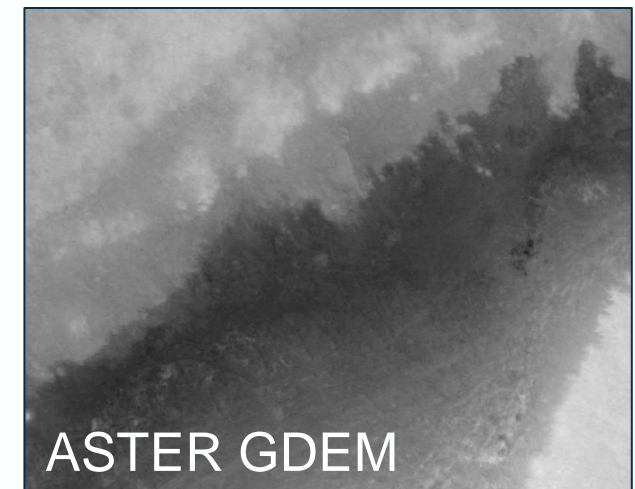
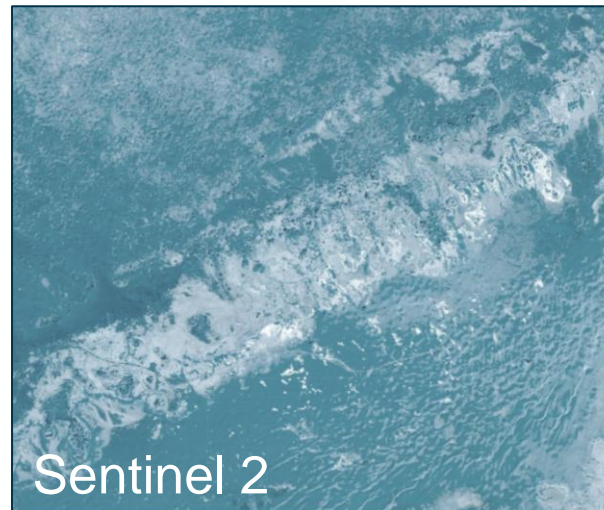
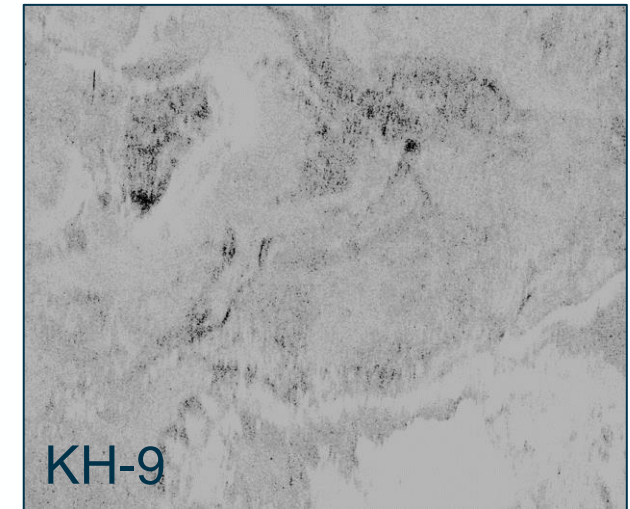
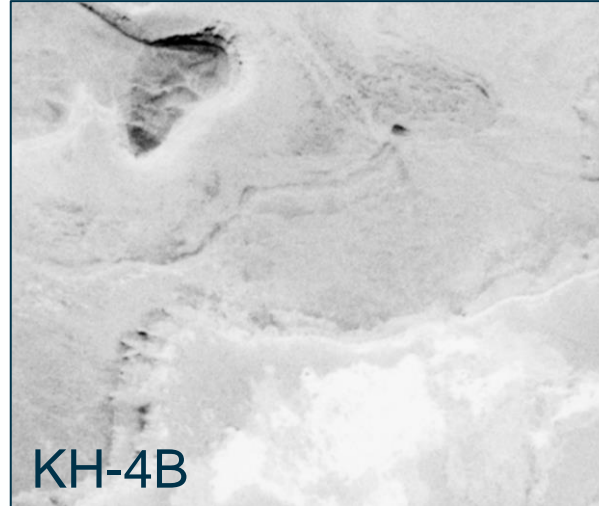
Hexagon KH-9

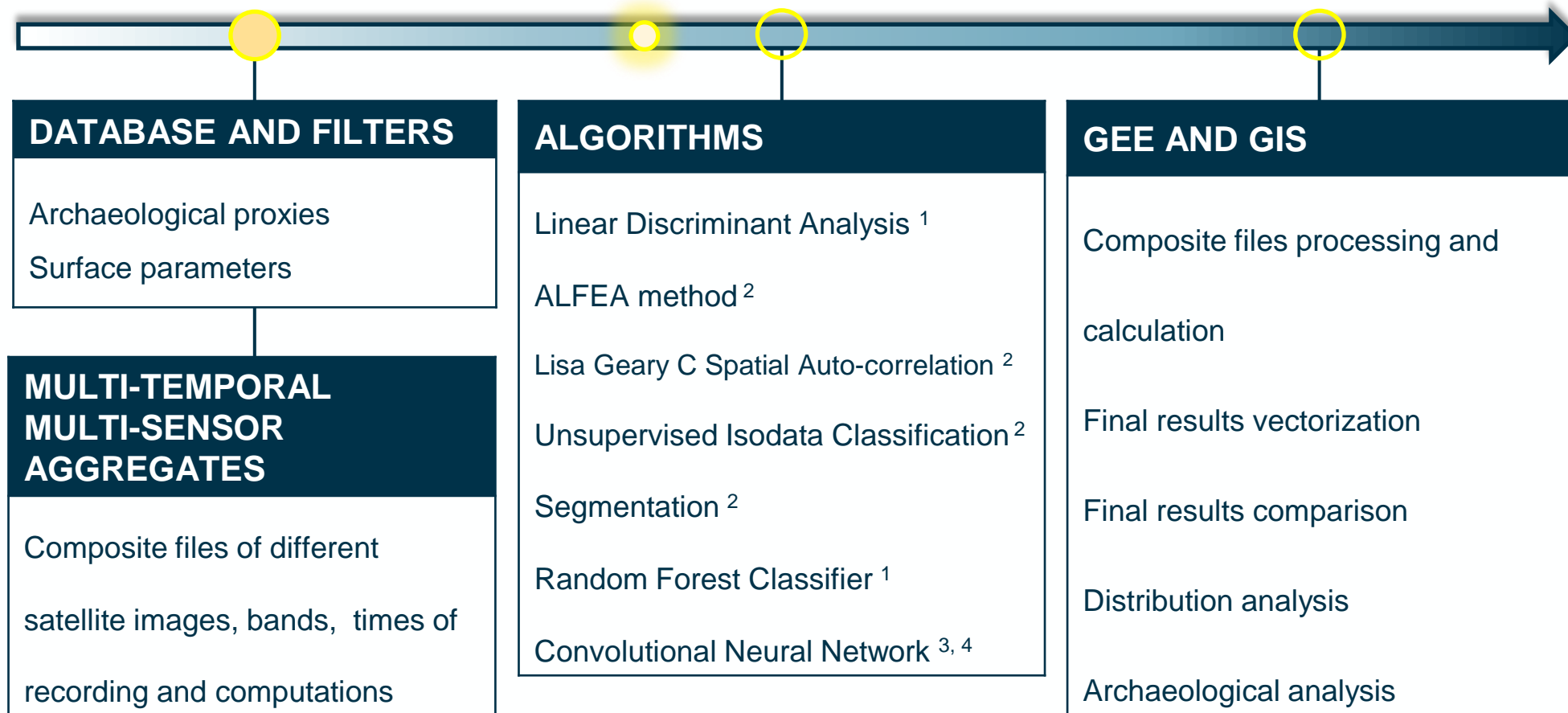
Sentinel 2

RGB, NIR, SWIR1, SWIR2

ASTER GDEM

(COSMO SkyMed, TanDEM-X)

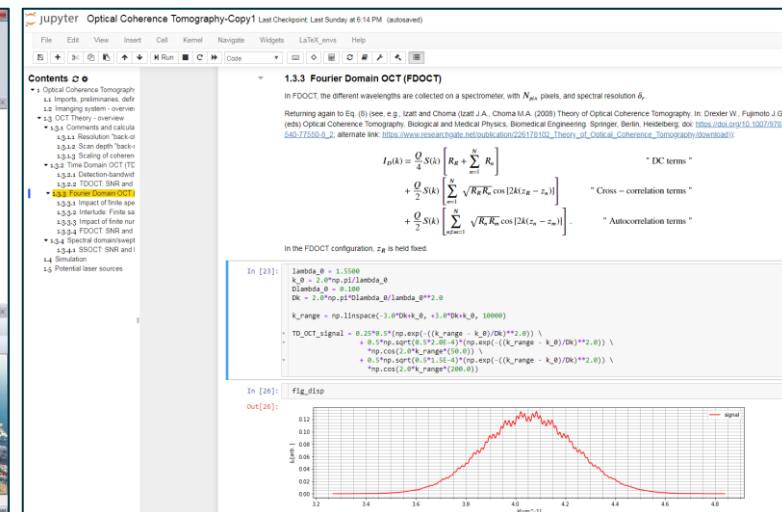
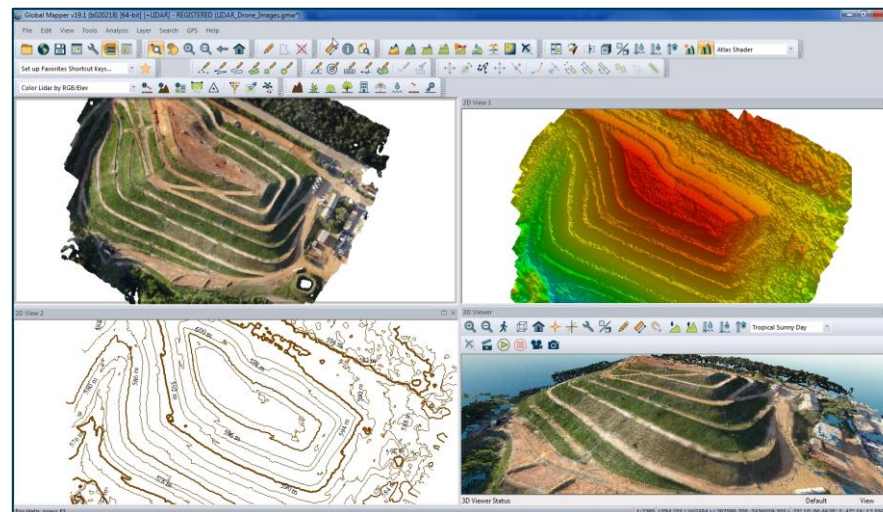
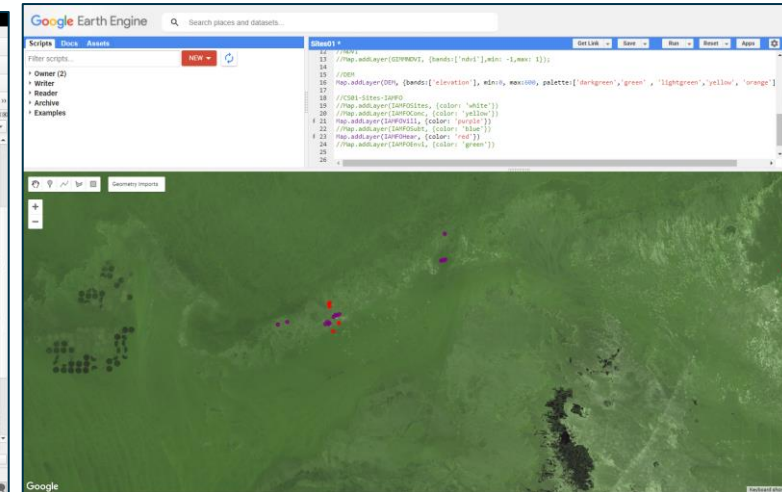
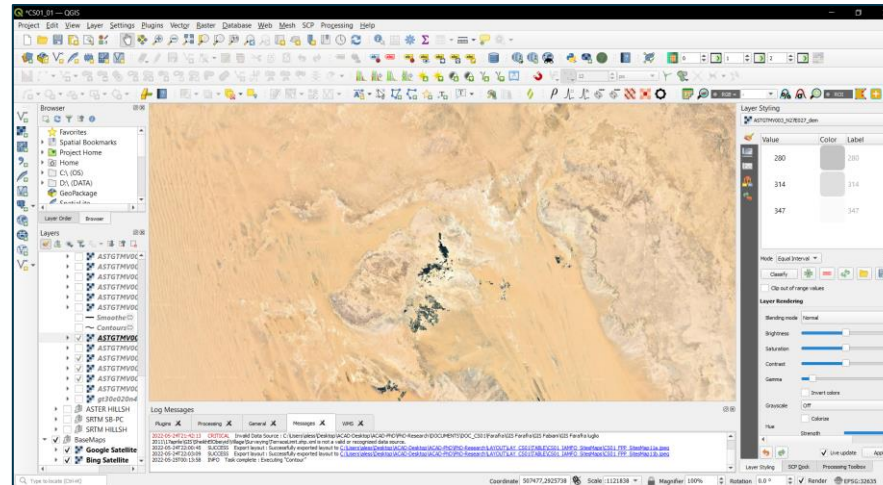




1. Orengo et al. 2020
2. Lasaponara et Masini 2018
3. Albawi et al. 2017
4. O'Shea et Ryan 2015
5. Costanzo et al. 2021

PLATFORMS

- GIS
- GEE
- Global Mapper
- Code editors



ARCHAEOLOGICAL PROXIES

Shadow marks

Feature morphology

Feature orientation

Construction materials

Environmental hotspots

Archaeological hotspots

Spectral signatures

SURFACE PARAMETERS

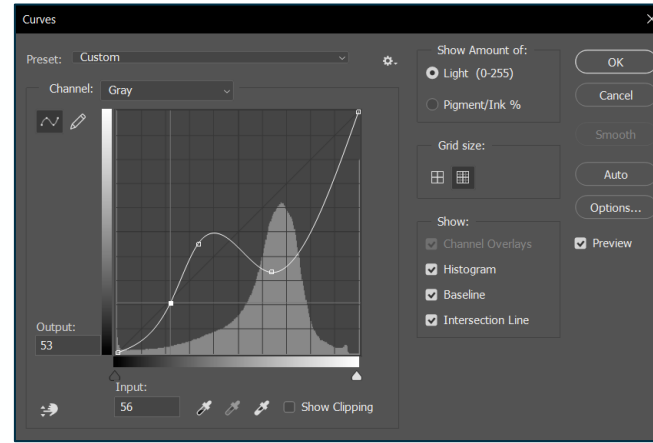
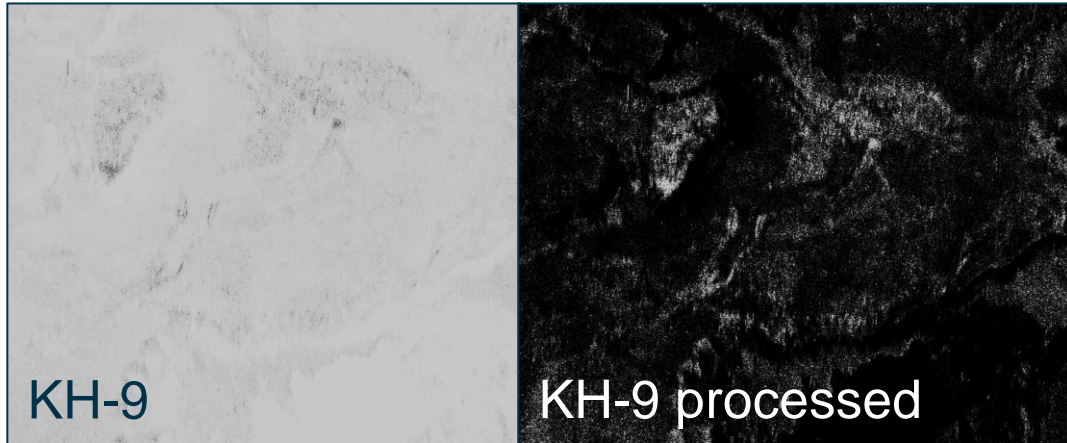
Surface roughness

Surface discontinuity

Paleo and modern topography,
hydrography and climatology

Electric conductivity of the soil

Moisture content percentage

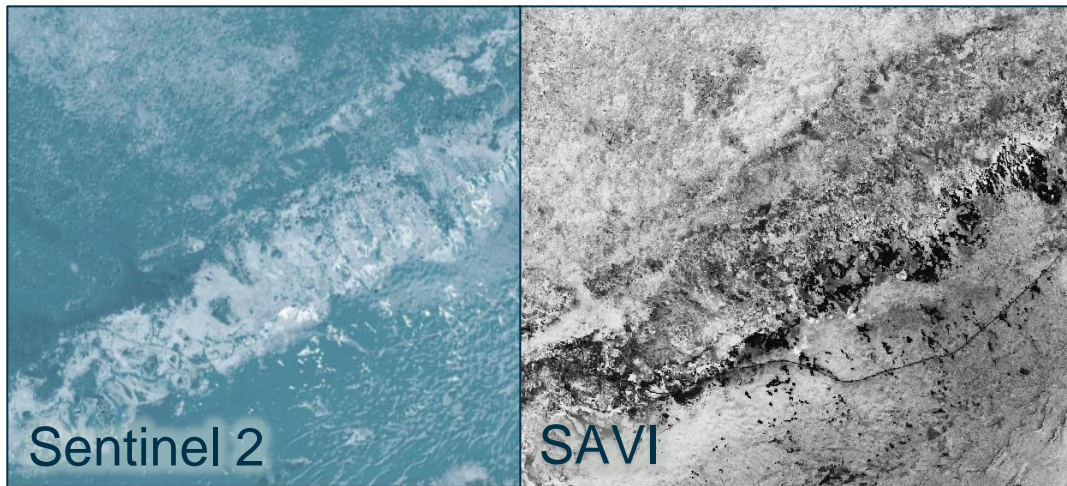


PROCESSES

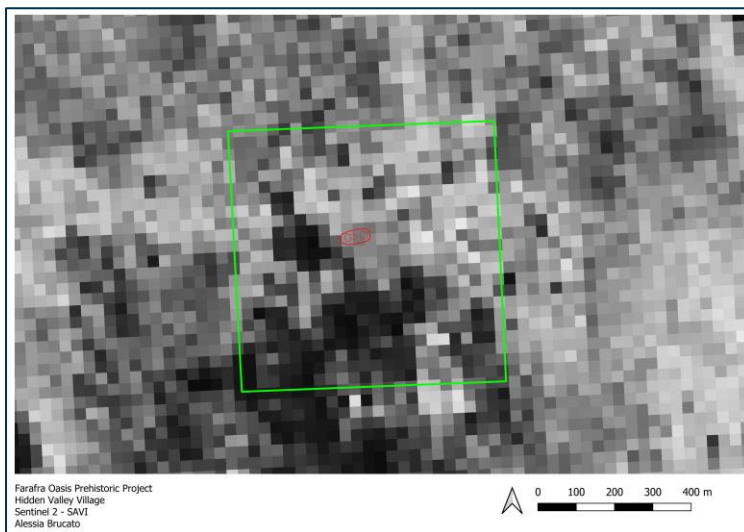
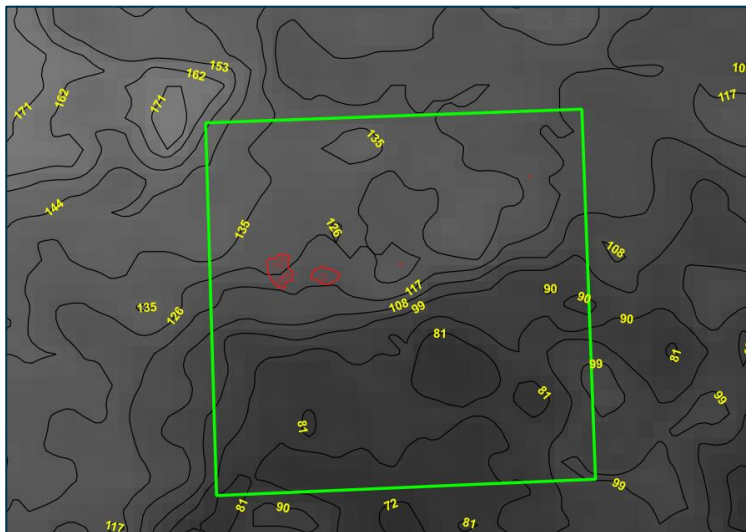
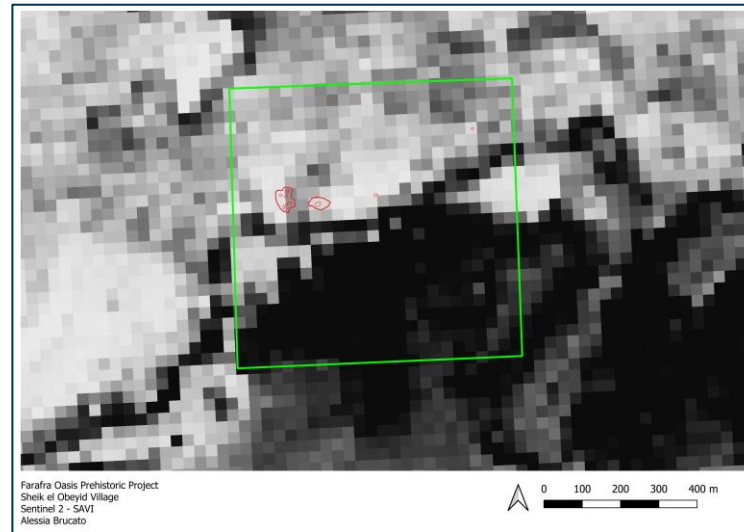
Color Curves calibration and noise reduction

Spectral Indices calculation

(Mean, PCA)



```
CS01_S2_SpectralIndices
200
201
202 // Green Normalized Difference Vegetation Index ----- GNDVI
203
204 var gndvi = (nir.subtract(green)).divide(nir.add(green)).rename('GNDVI');
205 var gndviParams = {min: 0.1164, max: 0.4928, palette: ['black', 'green', 'lightgreen', 'lightblue']};
206 Map.addLayer(gndvi, gndviParams, 'GNDVI');
207 print(gndvi, 'GNDVI');
208
209
210 // Green Ratio Vegetation Index ----- GVI
211
212 var gvi = nir.divide(green).rename('GVI');
213 var gviParams = {min: 1.2961, max: 1.9918, palette: ['black', 'green', 'lightgreen', 'lightblue']};
214 Map.addLayer(gvi, gviParams, 'GVI');
215 print(gvi, 'GVI');
216
217
218 // Green Vegetation Index ----- GVI
219
220 var gvi = (blue.multiply(-0.2848)).add(green.multiply(-0.2435)).add(red.multiply(-0.5436)).add(nir.multiply(1.2534)).rename('GVI');
221 var gviParams = {min: -1223.71, max: 148.25, palette: ['black', 'green', 'lightgreen', 'lightblue']};
222 Map.addLayer(gvi, gviParams, 'GVI');
223 print(gvi, 'GVI');
224
225
226 // Modified Chlorophyll Absorption in Reflectance ----- MCArI
227
228 var mcarl = (((nir.subtract(red)).multiply(2.5)).multiply(1.2)).subtract(nir.subtract(green)).multiply(1.2)).divide(nir.add(red)).rename('MCArI');
229 var mcarlParams = {min: 1134.71, max: 706.81, palette: ['black', 'green', 'lightgreen', 'lightblue']};
230 Map.addLayer(mcarl, mcarlParams, 'MCArI');
231 print(mcarl, 'MCArI');
232
233
234 // Modified Non-Linear Index ----- MNLi
235
236 var const2 = ee.Image.constant(0.5);
237 var mnl1 = (((nir.multiply(nir)).subtract(red)).multiply(const2.add(1)).divide(nir.multiply(nir))).multiply(1.2)).divide(nir.add(red)).rename('MNLi');
238 var mnl1Params = {min: 1.4991, max: 1.4996, palette: ['black', 'green', 'lightgreen', 'lightblue']};
239 Map.addLayer(mnl1, mnl1Params, 'MNLi');
240 print(mnl1, 'MNLi');
```



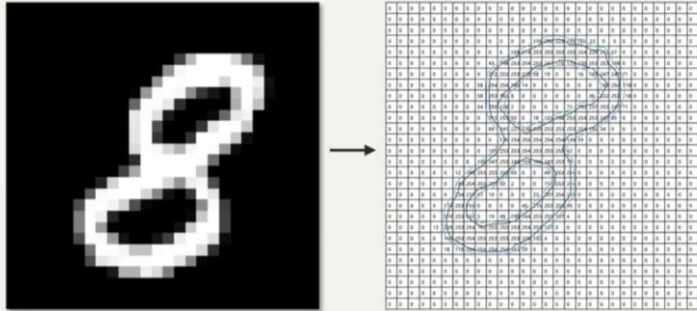
Multitemporal Multisensory
Overlapping Composites



Training vectors for ML:

- Slab Structures
- Proto-villages
- Surroundings

Images are Encoded as Numbers



Data Source: MNIST Dataset by LeCun et al. (1998) / CC-by-SA 3.0

Convolutional Neural Network Multiclass Perceptron

```
class Net(nn.Module):
    def __init__(self):
        super().__init__() # just run the init of parent class (nn.Module)
        self.conv1 = nn.Conv2d(1, 32, 5, padding=2) # input is 1 image, 32 output channels, 5x5
        self.conv2 = nn.Conv2d(32, 64, 5, padding=2) # input is 32, bc the first layer output 32
        self.conv3 = nn.Conv2d(64, 128, 5, padding=2) # input is 64, bc the first layer output 32 channels, 5x5 kernel / window

        self.fc1 = nn.Linear(128*25*25, 512) #flattening.
        self.fc2 = nn.Linear(512, 2) # 512 in, 2 out bc we're doing 2 classes (dog vs cat).

    def convs(self, x):
        # max pooling over 2x2
        x = F.max_pool2d(F.relu(self.conv1(x)), (2, 2))
        x = F.max_pool2d(F.relu(self.conv2(x)), (2, 2))
        x = F.max_pool2d(F.relu(self.conv3(x)), (2, 2))

        return x

    def forward(self, x):
        x = self.convs(x)
        x = x.view(-1, 128*25*25) # .view is reshape ... this flattens X before
        #x = torch.flatten(x, start_dim=0)
        x = F.relu(self.fc1(x))
        x = self.fc2(x) # bc this is our output layer. No activation here.
        return F.softmax(x, dim=1)

net = Net()
print(net)
device = torch.device("cuda:0")
#device = torch.device('cpu')
net.to(device)
if REBUILD_DATA:
    dogsvcats = DogsVSCats()
    dogsvcats.make_training_data()

training_data = np.load("training_data.npy", allow_pickle=True)
print(len(training_data))
```

```
class Net(nn.Module):
    def __init__(self):
        super().__init__() # just run the init of parent class (nn.Module)
        self.conv1 = nn.Conv2d(1, 32, 5, padding=2) # input is 1 image, 32 output channels,
        self.conv2 = nn.Conv2d(32, 64, 5, padding=2) # input is 32, bc the first layer output
        self.conv3 = nn.Conv2d(64, 128, 5, padding=2) # input is 64, bc the first layer output 32 channels, 5x5 kernel / window

        self.fc1 = nn.Linear(128*25*25, 512) #flattening.
        self.fc2 = nn.Linear(512, 2) # 512 in, 2 out bc we're doing 2 classes (dog vs cat).

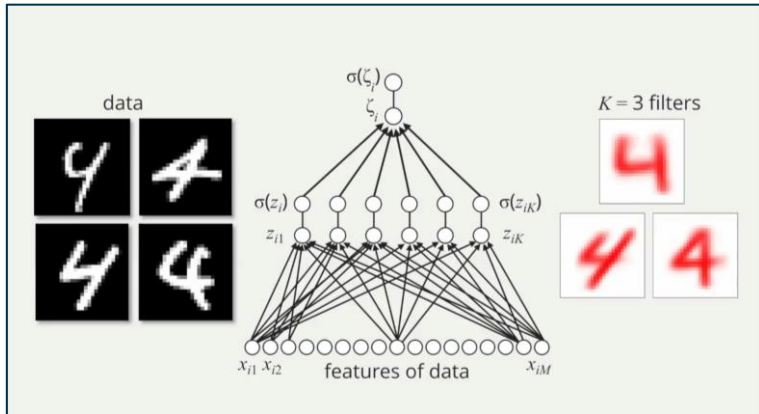
    def convs(self, x):
        # max pooling over 2x2
        x = F.max_pool2d(F.relu(self.conv1(x)), (2, 2))
        x = F.max_pool2d(F.relu(self.conv2(x)), (2, 2))
        x = F.max_pool2d(F.relu(self.conv3(x)), (2, 2))

        return x

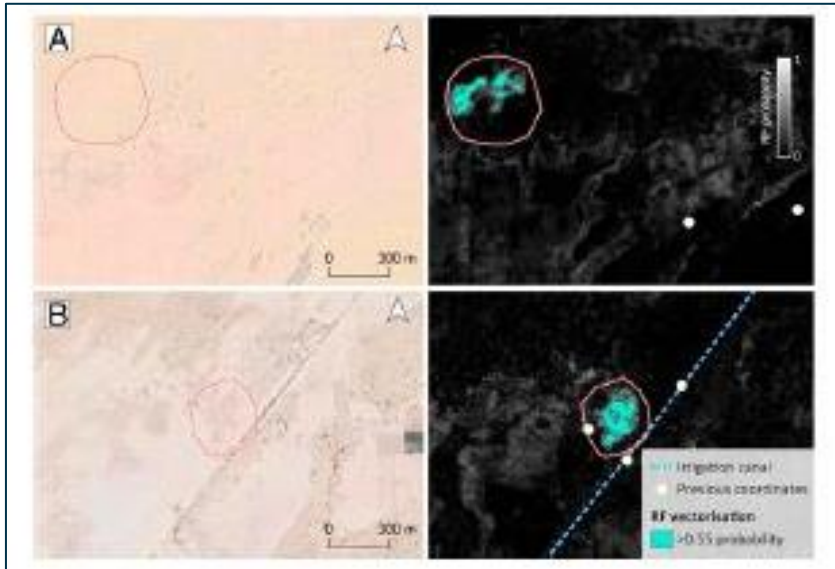
    def forward(self, x):
        x = self.convs(x)
        x = x.view(-1, 128*25*25) # .view is reshape ... this flattens X before
        #x = torch.flatten(x, start_dim=0)
        x = F.relu(self.fc1(x))
        x = self.fc2(x) # bc this is our output layer. No activation here.
        return F.softmax(x, dim=1)

net = Net()
print(net)
device = torch.device("cuda:0")
#device = torch.device('cpu')
net.to(device)
if REBUILD_DATA:
    dogsvcats = DogsVSCats()
    dogsvcats.make_training_data()

training_data = np.load("training_data.npy", allow_pickle=True)
print(len(training_data))
```



L. Carin , D. Carlson, T. Dunn, K. Liang,
Introduction to Machine Learning, Duke
University, Coursera



H.A. Orengo et al. 2020

The preliminary results of this study

- 1) are currently being collected and checked within a relational database and a GIS through Error Rate with Cross-Entropy Validation;
- 2) will enrich the existing archaeological datasets about the hunter-gatherer/early herder groups populating the EWD during the Early and Mid-Holocene;



- 3) will provide essential information about the human mobility patterns between the Eastern Sahara and the Nile Valley during the same period, shedding new light on the contribution of these communities to the emergence of the Egyptian late prehistoric and Predynastic cultures.

This study will offer an effective approach to overcome many difficulties of ground-based surveys, especially in Egypt where, after 2015, access to the EWD was reduced and denied by the Egyptian Authorities due to security and safety concerns.

In fact, despite the efforts of several international research groups to identify and assess the distribution of these features, right now it is impossible to bring to light new sites or study the known sites via traditional ground-based surveys.

The application of a remote, automated, precise, and cost-effective methodology for feature detection and analysis will help the archaeological research overcome these obstacles and open new lines of investigation.

- S. Albawi , T.A. Mohammed, S. Al Zawi , Understanding of a Convolutional Neural Network , in 2017 International Conference on Engineering and Technology (ICET), 2017, DOI: 10.1109/ICEngTechnol.2017.8308186
- M. Amani , A. Ghorbanian , S.A. Ahmadi , M. Kakooei , A. Moghimi , S.M. Mirmazloumi , S.H.A. Moghaddam , S. Mahdavi , M. Ghahremanloo , S. Parsian , Q. Wu , B. Brisco , Google Earth Engine Cloud Computing Platform for Remote Sensing Big Data Applications: A Comprehensive Review , in IEEE Journal of Selected Topics in Applied Earth Observations and Remote Sensing , 13, 2020
- B.E. Barich, G. Lucarini, M.A. Hamdan, F.A.Hassan, From Lake to sand. The Archaeology of Farafra Oasis, Western Desert Egypt, Monography 2014, ISBN: 978887145207
- R. Bennett, D. Cowley, V. De Laet , The data explosion : Tackling the taboo of automatic feature recognition in airborne survey data , in Antiquity 2014, 88, 896 905.
- I. Berganzo-Besga, H.A. Orenge, F. Lumbreras, M. Carrero-Pazos, J. Fonte, B. Vilas-Estévez. 2021. "Hybrid MSRM-Based Deep Learning and Multitemporal Sentinel 2-Based Machine Learning Algorithm Detects Near 10k Archaeological Tumuli in North-Western Iberia" Remote Sensing 13, no. 20: 4181. <https://doi.org/10.3390/rs13204181>
- J. Casana , Regional scale archaeological remote sensing in the age of big data. Automated site discovery vs. brute force methods in Advance in Archaeological Practice , 2(3), 222 233. doi:10.7183/2326 3768.2.3.222
- M.J. Harrower , J. Schuetter , J. Mccorriston , P.K. Goel , M.J. Senn , Survey, Automated Detection , and Spatial Distribution Analysis of Cairn Tombs in Ancient Southern Arabia. In Mapping Archaeological Landscapes from Space , in Mapping Archaeological Landscapes from Space 2013, 259 268, DOI: 10.1007/978 1 4614 6074 9_22
- K. Kvamme , An examination of automated archaeological feature recognition in remotely sensed imagery . In Computational Approaches to Archaeological Spaces ; Bevan , in Computational Approaches to Archaeological Spaces , 2020; pp.53 68.
- R. Lasaponara , N. Masini, Space Based Identification of Archaeological Illegal Excavations and a New Automatic Method for Looting Feature Extraction in Desert Areas , in Surveys in Geophysics 2018, 39, 1323 1346, <https://doi.org/10.1007/s10712 018 9480 4>
- R. Lasaponara, N. Abate and N. Masini. 2022. "On the Use of Google Earth Engine and Sentinel Data to Detect "Lost" Sections of Ancient Roads. The Case of Via Appia" IEEE Geoscience and Remote Sensing Letters 19, no. 3001605: 1-5. <https://doi.org/10.1109/LGRS.2021.3054168>.
- G. Lucarini. 2011. "Il Paesaggio Antico di Sheikh el Obeiyid (Farafra). La Playa e il Villaggio tra Tecnologia e Aspetti Simbolici" Scienze dell'Antichità 17: 45-60. Permalink: <http://digital.casalini.it/3086888>
- N. Masini, R. Lasaponara , Sensing the Past from Space: Approaches to site detection . Sensing the Past , in Geotechnologies and the Environment, 2017, 16, 23 60, https://doi.org/10.1007/978 3 319 50518 3_2
- N. Masini, R. Lasaponara , Recent and Past Archaeological Looting by Satellite Remote Sensing: Approach and Application in Syria , in Remote Sensing for Archaeology and Cultural Landscapes 2020, 123 137, https://doi.org/10.1007/978 3 030 10979 0_8
- H.A. Orenge, F.C. Conesa , A. Garcia Molsosa , A. Lobo, A.S. Green, M. Madella , C.A. Petrie , Automated detection of archaeological mounds using machine learning classification of multisensor and multitemporal satellite data , in Proceedings of the National Academy of Science of the United States of America , PNAS 2020, 117, 31, 2020, pp. 18240 18250
- K. O'Shea, N. Ryan , An Introduction to Convolutional Neural Networks , in ArXiv e prints , 2015, DOI: arXiv:1511.08458 [cs.
- L. Rayne , J. Bradbury, D. Mattingly, G. Philip, R. Bewley , A. Wilson, From Above and on the Ground: Geospatial Methods for Recording Endangered Archaeology in the Middle East and North Africa , in Geosciences 2017, 7, 100, 1 31, doi:10.3390/geosciences7040100
- D. Tapete , F. Cigna, Donoghue , D.N.M., Looting marks ' in space borne SAR imagery : Measuring rates of archaeological looting in Apamea (Syria) with TerraSAR X Staring Spotlight , in Remote sensing of environment , 178, 42 581

THANK YOU



UNIONE EUROPEA
Fondo Sociale Europeo
Fondo Europeo di Sviluppo Regionale



*Ministero dell'Istruzione,
dell'Università e della Ricerca*



ISMEO

Thank you

